Hyaluronic acid–bilirubin nanomedicine for targeted modulation of dysregulated intestinal barrier, microbiome and immune responses in colitis

Yonghyun Lee [1,2,3], Kohei Sugihara[4], Merritt G. Gillilland III[4], Sangyong Jon [5], Nobuhiko Kamada[4] and James J. Moon [1,2,3]*

While conventional approaches for inflammatory bowel diseases mainly focus on suppressing hyperactive immune responses, it remains unclear how to address disrupted intestinal barriers, dysbiosis of the gut commensal microbiota and dysregulated mucosal immune responses in inflammatory bowel diseases. Moreover, immunosuppressive agents can cause off-target systemic side effects and complications. Here, we report the development of hyaluronic acid–bilirubin nanomedicine (HABN) that accumulates in inflamed colonic epithelium and restores the epithelium barriers in a murine model of acute colitis. Surprisingly, HABN also modulates the gut microbiota, increasing the overall richness and diversity and markedly augmenting the abundance of *Akkermansia muciniphila* and *Clostridium* XIVα, which are microorganisms with crucial roles in gut homeostasis. Importantly, HABN associated with pro-inflammatory macrophages, regulated innate immune responses and exerted potent therapeutic efficacy against colitis. Our work sheds light on the impact of nanotherapeutics on gut homeostasis, microbiome and innate immune responses for the treatment of inflammatory diseases.

Pathogenesis of inflammatory bowel diseases (IBDs) is associated with disrupted intestinal barrier functions[1,2], imbalance of the gut microbiome[3–5] and subsequent dysregulated mucosal immune responses to gut commensal bacteria[3–5]. Traditional medical interventions for IBDs have mainly focused on managing the symptoms of IBDs by suppressing immune responses[6]; however, they generally do not address the underlying causes of IBDs, including damage to the mucus layer in the gastrointestinal tract, subsequent loss of intestinal barrier functions and dysbiosis of the gut commensal microorganisms. Moreover, despite advances in localized drug delivery[7–9], conventional immunosuppressive drugs based on small molecules or biologics can cause off-target systemic side effects, and their long-term use may lead to serious complications, such as opportunistic infections, malignancies, autoimmunity and liver toxicity[6,10]. Towards the goal of addressing this unmet medical need, we have developed a nanotherapeutic platform that can target inflamed colonic epithelium, modulate the gut microbiome and promote anti-inflammatory immune responses in local tissues, with improved efficacy compared with traditional IBD therapeutics in a murine model of acute colitis.

We have designed a HABN system that is formed by nano-aggregation of an amphiphilic conjugate between hyaluronic acid (HA) and bilirubin. HA, which is a glycosaminoglycan biopolymer commonly found in synovial fluid and extracellular matrix, has immunomodulatory properties, including regulation of macrophages[11], induction of antimicrobial peptides[12] and regulatory CD4+ T (T_reg) cells[13]. While free HA or HA-based nanoparticles have been explored for treating IBDs[14,15], their efficacy has been hampered by hyaluronidase-mediated rapid turnover of HA and the harsh oxidative conditions in inflamed colon[14,16]. On the other hand,

bilirubin (BR), a hydrophobic byproduct of haemoglobin breakdown found in bile, has strong reactive oxygen species (ROS)-scavenging, anti-oxidant and cytoprotective properties[17,18]; however, its clinical development has been limited due to its hydrophobicity and toxicity, and it remains unknown how to exploit the salient features of BR for treating local inflamed tissues, such as damaged colon in IBDs.

Here we show that while BR is practically insoluble in water, the HA shell permits aqueous formulation of BR and allows targeting of orally administered HABN to inflamed colonic epithelium and pro-inflammatory macrophages via HA−CD44 interactions. Moreover, the BR core confers HABN with hyaluronidase resistance and potent ROS-scavenging capacity, protecting colonic epithelial cells against apoptosis in a murine model of dextran sulfate sodium (DSS)-induced acute colitis—a widely used model with clinical and histological features of human ulcerative colitis, including intestinal inflammation, loss of epithelium barrier functions, dysregulated host innate immunity and gut microbiome, severe bleeding and finally mortality[19]. Unexpectedly, our studies reveal that HABN modulates the gut microbiota, increasing its richness and diversity, and restores the expression of tight junction-associated proteins and intestinal barrier functions, thereby exerting strong anti-inflammatory effects against acute colitis.

ROS-scavenging HABN accumulates in inflamed colon
Specifically, we constructed a series of HA−BR polymers (Fig. 1a and Supplementary Fig. 1) and confirmed the synthesis of HA−BR conjugates using NMR (Supplementary Fig. 2). Whereas BR was insoluble in water, HA−BR conjugates with an average conjugation density of ~4 molecules of BR per each 100 kDa HA molecule were

---

[1]Department of Pharmaceutical Sciences, University of Michigan, Ann Arbor, MI, USA. [2]Department of Biomedical Engineering, University of Michigan, Ann Arbor, MI, USA. [3]Biointerfaces Institute, University of Michigan, Ann Arbor, MI, USA. [4]Division of Gastroenterology, Department of Internal Medicine, University of Michigan, Ann Arbor, MI, USA. [5]KAIST Institute for the BioCentury, Department of Biological Sciences, Korea Advanced Institute of Science and Technology, Daejeon, Republic of Korea. *e-mail: moonjj@umich.edu

readily dispersed in aqueous buffer (Supplementary Fig. 3a,b). As shown by transmission electron microscopy (TEM) and dynamic light scattering measurements, HA−BR conjugates in aqueous buffer self-assembled to form HABN (Fig. 1a). As the molecular weight (M_W) of HA increased from 10 kDa (10 K HA) to 700 kDa (700 K HA), the hydrodynamic size of HABN increased from 86 ± 5 nm to 416 ± 9 nm, and its zeta potential decreased from -35.6 ± 1.6 mV to -46.2 ± 5.2 mV, respectively (Supplementary Fig. 3c,d). HABN exhibited significant ROS-scavenging activity ($P < 0.0001$, compared with HA and HAoxBR, an oxidized form of HABN, Fig. 1b) and protected human HT-29 colonic epithelial cells from ROS-mediated cytotoxicity (Fig. 1c). HABN rapidly dissociated on exposure to ROS in the presence of a free radical, NaOCl, or a peroxy radical generator, 2,2'-Azobis(2-amidinopropane) dihydrochloride (AAPH; Supplementary Figs. 4 and 5). In contrast, control nanoparticles self-assembled from HA−cholesterol conjugates (HACN) did not exhibit ROS-responsiveness (Supplementary Figs. 6–8) and failed to protect HT-29 cells from ROS (Fig. 1c), suggesting a crucial role of BR in the cytoprotective effect of HABN. In addition, HABN was significantly more resistant to hyaluronidase-mediated degradation, compared with free HA (Fig. 1d), potentially due to steric hindrance from self-assembled nanostructures.

Importantly, in mice given 3% DSS in drinking water as an acute model of colitis, orally administered Cy5.5-conjugated HABN nanoparticles (HABN−Cy5.5; as well as Cy5.5-conjugated HACN nanoparticles (HACN−Cy5.5)) accumulated in DSS-inflamed colon and associated with F4/80+ macrophages in the colonic mucosa within 6 h (Fig. 1e–g and Supplementary Figs. 9 and 10); however, HABN was not detected in the colon of healthy mice (Fig. 1e−g). When HABN was incubated with murine lamina propria mononuclear cells in vitro, HABN was taken up by macrophages (CD11b+CD11c+ and CD11b+CD11c−) and granulocytes (CD11b+CD11c−Ly6G+) (Supplementary Fig. 11). When incubated with M0/M1/M2 J774A.1 macrophages in vitro, HABN was strongly associated with pro-inflammatory M1 macrophages, with minimal signal from conventional M0 or M2 macrophages (Supplementary Fig. 12a,c). Pretreatment of M1 macrophages with either free HA or antibody against its known receptor, CD44, abrogated HABN signal (Supplementary Fig. 12b,d), suggesting CD44-mediated association of HABN in macrophages.

Efficacy against colitis and comparison with other IBD drugs

We next evaluated the therapeutic efficacy of HABN against DSS-induced acute colitis. We first examined whether the M_W of HA influenced the therapeutic outcomes of HABN since the M_W of HA is known to modulate pro- and anti-inflammatory responses[16]. C57BL/6 mice were given 3% DSS in drinking water for 6 d, and various HABN formulations were administered via oral gavage on days 0, 2, 4 and 6. Compared with PBS, 100K HABN treatment significantly protected animals against DSS-induced bodyweight loss and shortening of colon length, while suppressing colonic tissue damage, immune cell infiltration and IBD-associated myeloperoxidase (MPO) activity in colon[20] (Supplementary Fig. 13). In contrast, mice treated with 10K HABN or 700K HABN did not achieve full bodyweight recovery and a subset of animals had shortened colon length.

Based on the promising outcomes of 100K HABN, we directly compared its efficacy against free 100K HA, 100K HACN, as well as PEG−BN, a control nanoparticle group with the HA moiety switched to PEG (Supplementary Figs. 14 and 15, and Fig. 2a). Whereas DSS-colitis mice treated with HABN quickly recovered their bodyweight, other control treatment groups failed to prevent the bodyweight loss (Fig. 2b). Furthermore, colon length in the HABN group was similar to that in healthy mice and significantly longer than that in other treatment groups ($P < 0.01$, Fig. 2c). HABN treatment also protected colonic epithelium against

pathological damage and suppressed the MPO activity ($P < 0.001$, compared with PBS, Fig. 2d,e). Furthermore, HAoxBR failed to protect animals against DSS-induced colitis (Supplementary Fig. 16). These studies suggest that the efficacy of HABN was derived in part by both HA and BR.

We next directly compared the efficacy of HABN against other conventional IBD therapeutics widely used in the clinic, including 5-aminosalicyclic acid (5-ASA), methylprednisolone (MPS) and dexamethasone (DEX)[6]. Compared with 5-ASA, MPS and DEX used at their clinical doses, HABN treatment exhibited significantly enhanced efficacy against DSS-induced acute colitis, achieving full bodyweight recovery, maintaining colon length and reducing colonic damage and MPO activity (Fig. 2f–j). Unlike small molecule drugs, such as MPS known for systemic side effects including thymic involution[21], HABN treatments did not trigger any overt signs of systemic toxicity, autoimmunity or pathologies in the major organs (Supplementary Figs. 17 and 18). We also confirmed that the free mixture of HA and bilirubin (HA+BR) had minimal therapeutic effect (Fig. 2f–j). Taken together, HABN formed by self-assembled conjugates of HA and bilirubin protected animals against colitis in an effective and safe manner.

Restoration of colonic epithelium

Intrigued by these results, we examined the impact of HABN on DSS-inflamed colonic epithelium with disrupted intestinal barrier functions[1,2]. DSS-colitis mice orally administered with HABN normalized the expression patterns and messenger RNA levels of ZO-1 and occludin-1, which are tight junction-associated proteins that play pivotal roles in gut homeostasis[2] (Fig. 3a,b); however, other control groups, including free HA, HACN, PEG−BN and HA+BR treatment, had minimal impact. Furthermore, compared with other treatments, HABN prevented systemic exposure of fluorescein isothiocyanate (FITC)-dextran after oral administration in DSS-colitis mice ($P < 0.001$, Fig. 3c), demonstrating restoration of intestinal barrier functions. HABN also induced the expression of antimicrobial peptides, including murine β-defensin 3 in vivo (Fig. 3d). When tested in the DSS-induced model of colitis associated with ROS-mediated colonic damage[22], HABN treatment markedly reduced the level of apoptosis in the colonic epithelium, as shown by the terminal deoxynucleotidyl transferase dUTP nick end labelling (TUNEL) assay (Fig. 3e). Furthermore, HABN treatment significantly reduced the local levels of pro-inflammatory cytokines, such as interleukin (IL)-1β, tumour-necrosis factor (TNF)-α and IL-6 (Fig. 3f), while increasing the levels of anti-inflammatory IL-10 and transforming growth factor (TGF)-β cytokines (Fig. 3g). Moreover, HABN treatment significantly decreased the frequencies of pro-inflammatory CD11b+Ly6C+Ly6G− monocytes and CD11b+Ly6C+Ly6G+ neutrophils in lamina propria of DSS-colitis mice, while increasing the frequencies of anti-inflammatory CD11b+Ly6CLy6G−MHCII+ tissue-resident macrophages, CD3+CD4+Foxp3+ regulatory T cells and MHCII+CD11c+CD11b− dendritic cells (DCs) (Supplementary Fig. 19). Notably, HABN-mediated induction of IL-10 and TGF-β was only transient and returned to the basal levels after 10 d of stopping HABN treatment, and DSS-colitis mice treated with HABN lost the ability to accumulate HABN in colon (Supplementary Figs. 20 and 21), suggesting normal recovery of the colon tissue.

Modulation of gut microbiome

Emerging evidence suggests the influence of gut microbiome on IBDs[3–5] as well as the impact of bile organic compounds and polysaccharides on intestinal microbiota[23,24]. Thus, we examined whether HABN treatment modulated the composition of gut microbiota in DSS-colitis mice. Analyses of faecal samples by 16S ribosomal RNA gene sequencing in the V4 regions showed that HABN treatment significantly improved bacterial richness (observed operational taxonomic unit (OTU) richness) and diversity (Shannon
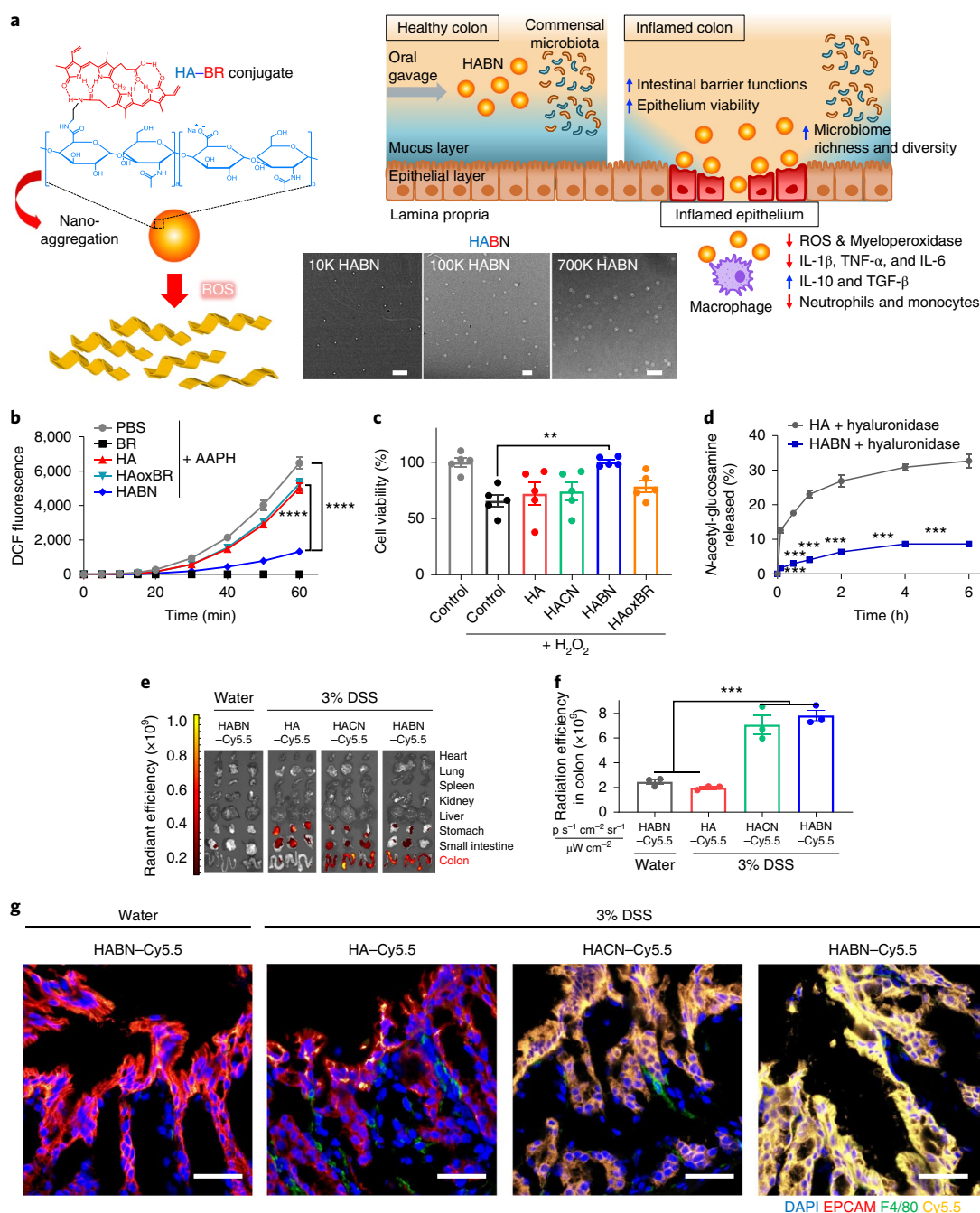
Fig. 1 | HABN localizes in inflamed colon in DSS-treated mice. a, Schematic of HABN self-assembled from HA−BR and their TEM images. HABN accumulates in inflamed colon and exerts therapeutic effects against acute colitis. Scale bars, 500 nm (10K HABN), 300 nm (100K HABN) and 400 nm (700K HABN). **b**, Fluorescence signals of DCF oxidized from DCFDA (50 µM) by peroxy radicals generated from 1 mM of AAPH at 37 °C in the presence of BR (50 µM), HA (1 mg ml^{-1}), HABN (1 mg ml^{-1}) or PBS. **c**, Viability of HT-29 cells was measured with CCK-8 assay after overnight treatment with 500 µg ml^{-1} of HA, HACN, HABN, HAoxBR or PBS in the presence of 100 µM H_2O_2. **d**, Generation of N-acetyl-glucosamine after treatment of 1 mg ml^{-1} HA or HABN with 100 IU ml^{-1} HYAL-II. **e,f**, After 6 h of treating animals with 7.5 mg kg^{-1} of HA−Cy5.5, HACN−Cy5.5 or HABN−Cy5.5, their organs were imaged by in vivo imaging system (IVIS) (**e**) and quantified for Cy5.5 fluorescence signal (**f**). **g**, Healthy or DSS-colitis mice were orally administered on day 6 with 7.5 mg kg^{-1} of HA−Cy5.5, HACN−Cy5.5 or HABN−Cy5.5 (equivalent mass of Cy5.5), and colon tissues were excised after 6 h, stained with anti-F4/80 and anti-EpCAM antibodies and visualized by confocal microscopy. Scale bars, 40 µm. Shown are representative images from six slides with n = 3 animals from two independent experiments. Data are presented as mean ± s.e.m. from a representative experiment (n = 5 biologically independent samples for **b**–**d** and n = 3 biologically independent animals for **e**–**g**) from two independent experiments. *$P < 0.05$, **$P < 0.01$, ***$P < 0.001$, ****$P < 0.0001$, analysed by one-way (**c,f**) or two-way (**b,d**) ANOVA with Tukey's HSD multiple comparison post hoc test.

and inverse-Simpson indices) in DSS-colitis mice, compared with other control groups (Fig. 4a,b). The non-metric multidimensional scaling (NMDS) plots revealed that DSS-colitis mice treated with HABN had distinct gut microbiota profile, compared with other treatment groups (Fig. 4c). Further analysis at the phylum/family level showed that HABN treatment significantly increased the
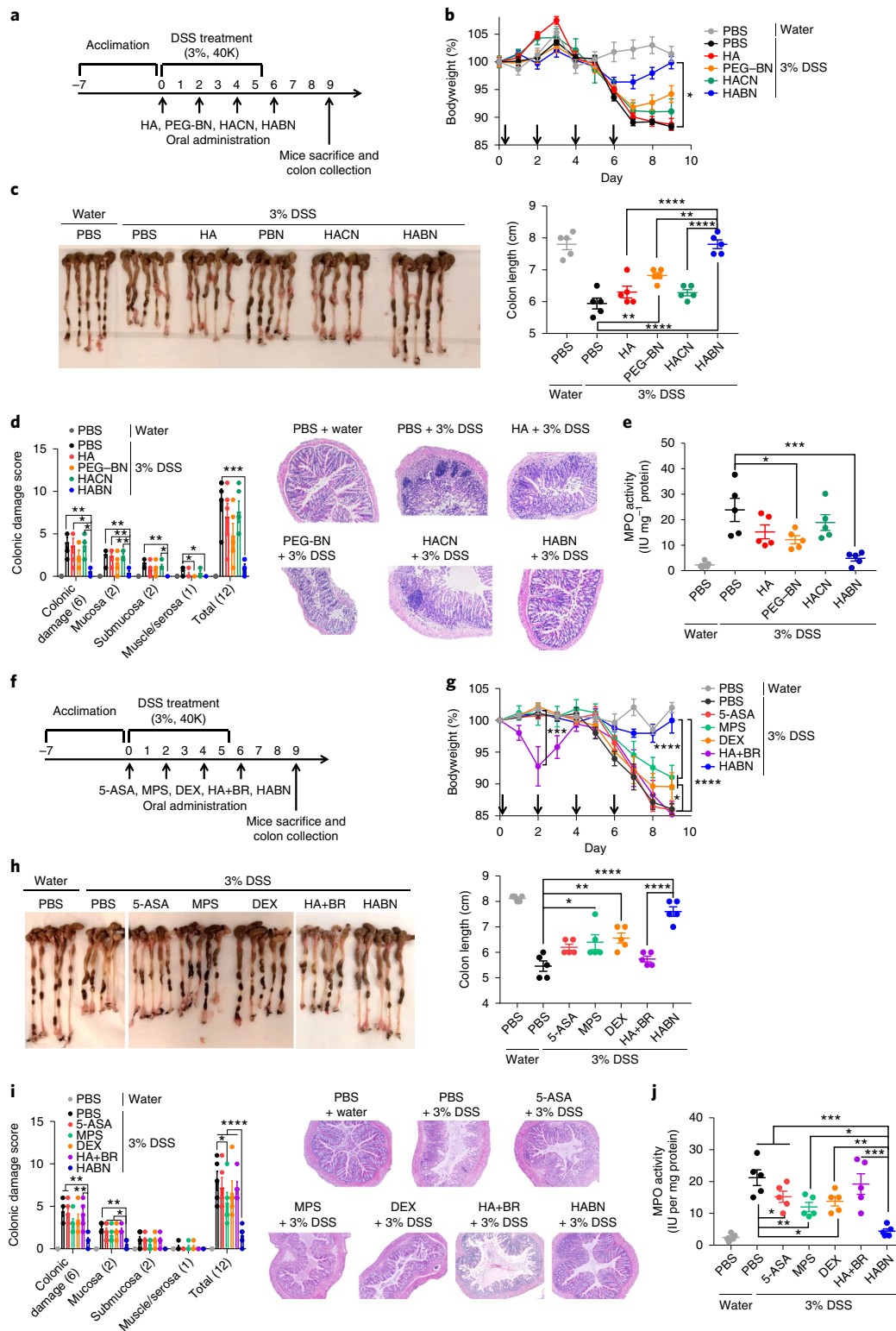
Fig. 2 | HABN exerts strong efficacy in a murine model of colitis. a, C57BL/6 mice were provided with water or 3% DSS-containing water for 6 d. On days 0, 2, 4 and 6, mice were orally administered with PBS or 30 mg kg⁻¹ of HA, HACN, HABN (with 100K HA at equivalent mass) or PEG–BN (equivalent mass of bilirubin as in HABN). **b**, Daily bodyweight changes in each group for 9 d. **c**–**e**, On day 9, animals were euthanized and colon length (**c**), colonic damage scores (**d**) and colonic MPO activity (**e**) were measured. **f**, C57BL/6 mice were provided with water or 3% DSS-containing water for 6 d. On days 0, 2, 4 and 6, mice were orally administered with PBS or 5-ASA (30 mg kg⁻¹), MPS (1 mg kg⁻¹), DEX (1 mg kg⁻¹), HA + BR (equivalent mass of bilirubin and HA as in HABN) or HABN (with 100K HA at equivalent mass, 30 mg kg⁻¹). **g**, Daily bodyweight changes in each group for 9 d. **h**–**j**, On day 9, animals were euthanized and colon length (**h**), colonic damage scores (**i**) and colonic MPO activity (**j**) were measured. Data are presented as mean ± s.e.m. from a representative experiment (*n* = 5 biologically independent animals) from four independent experiments (**a**–**e**) or two independent experiments (**f**–**j**). *$P < 0.05$, **$P < 0.01$, ***$P < 0.001$, ****$P < 0.0001$, analysed by one-way (**c**,**d**,**e**,**h**,**i**,**j**) or two-way (**b**,**g**) ANOVA with Tukey's HSD multiple comparison post hoc test.
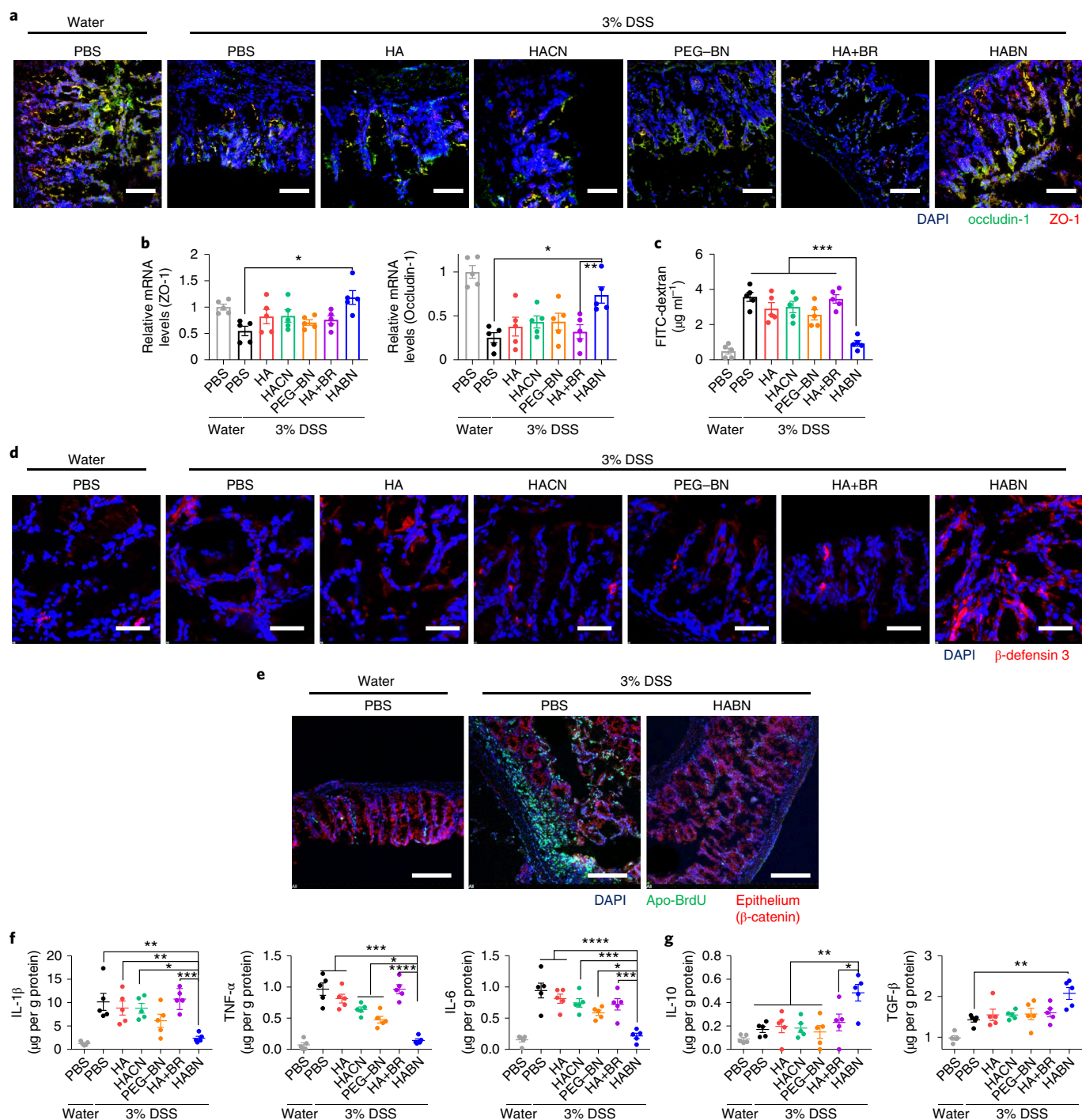
Fig. 3 | HABN protects colonic epithelium. a,b, Healthy or DSS-colitis mice were orally administered on day 0, 2, 4 and 6 with PBS or 30 mg kg⁻¹ of HA, HACN, PEG–BN, HA+BR or HABN (equivalent mass of HA and bilirubin), and colon tissues were excised and analysed for the expression patterns (**a**) and mRNA levels (**b**) of ZO-1 and occludin-1. **c,** Intestinal barrier functions were assessed in these mice by oral gavage of 4 kDa FITC-dextran on day 9, followed by measuring the FITC-dextran signal in blood after 4 h. **d,** Expression pattern of beta-defensin 3 was visualized by confocal microscopy. **e,** Colon tissues from healthy or DSS-colitis mice treated as shown were processed by the TUNEL assay, followed by visualization by confocal microscopy. Scale bars,100 μm (**a, d**), 50 μm (**e**). **f,g,** On day 9, colon tissues were analysed for the concentrations of pro-inflammatory (**f**) and anti-inflammatory (**g**) cytokines. Shown are representative images from ten slides with $n = 5$ biologically independent animals from two independent experiments. Data are presented as mean ± s.e.m. *$P < 0.05$, **$P < 0.01$, ***$P < 0.001$ and ****$P < 0.0001$, analysed by one-way ANOVA with Tukey's HSD multiple comparison post hoc test.

relative abundance of *Akkermansia muciniphila* (known to be associated with protective intestinal barrier functions[25–27]), *Clostridium* XIVα (known to induce T_reg cells[28]) and *Lactobacillus* (known for beneficial roles in both IBD animal models[29–31] and patients with

IBDs[32–35]) (Fig. 4d–f), which are all key factors that are prominently decreased in patients with IBDs[28,32,36,37]. Interestingly, when we pretreated DSS mice with broad-spectrum oral antibiotics, known to disrupt gut commensal microbes[38], this resulted in significantly
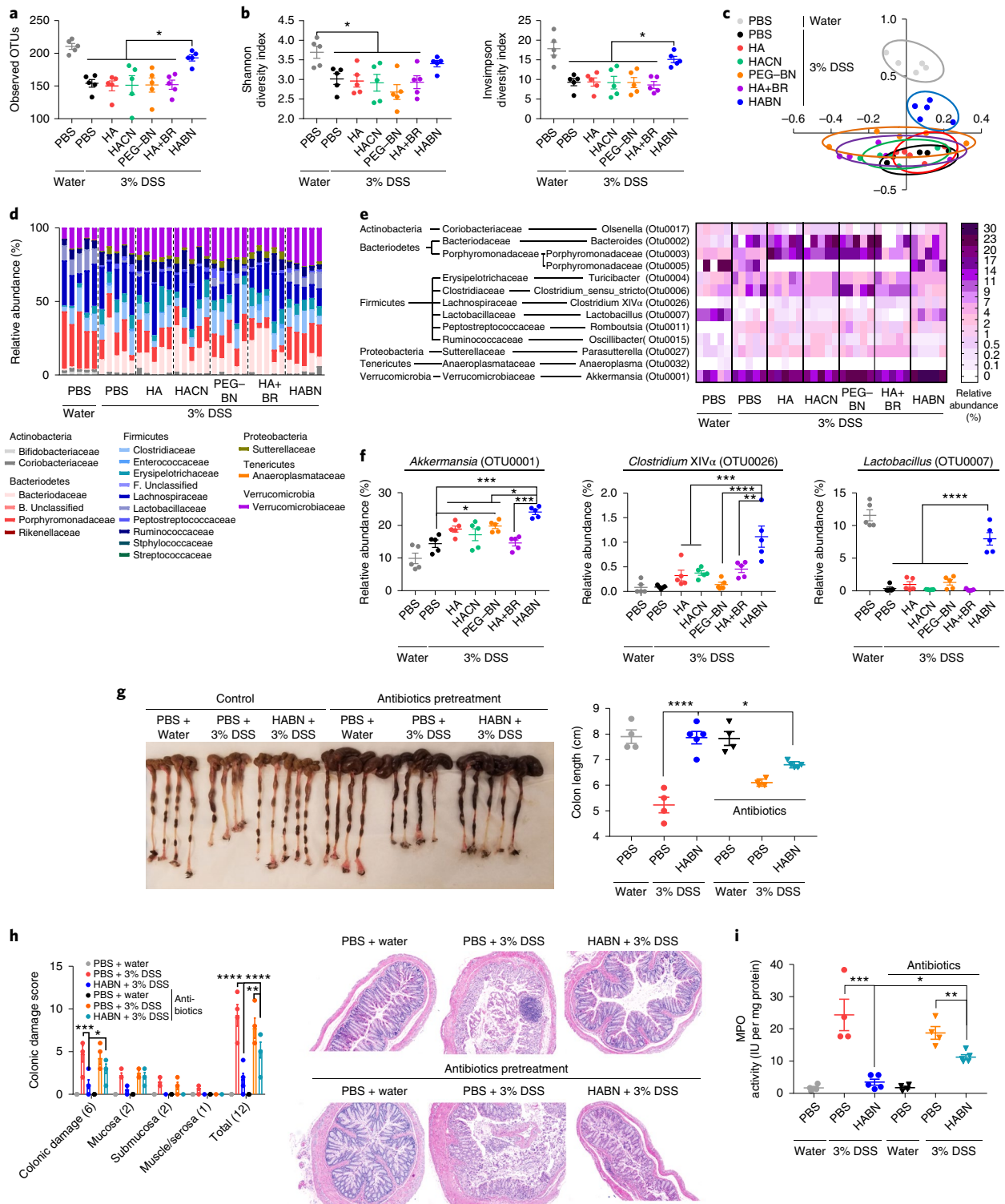
Fig. 4 | HABN alters the composition of gut microbiome. a–f, C57BL/6 mice were provided with 3% DSS in drinking water for 6 d. Mice were treated as above in Fig. 3. Faeces collected on day 9 were analysed for gut microbiome by 16S rRNA sequencing. **a,b**, Estimation of microbial community observed OTU richness (**a**) and α-diversity (**b**) (Shannon and inverse-Simpson indices). **c**, NMDS plot illustrating the gut microbiome β-diversity. Each point represents each mouse, based on a subsample of 1,122 OTU. **d**, Relative abundance of gut microbiome. Phylum- and family-level taxonomy are presented as a percentage of total sequences. **e**, Heatmap of the relative abundance of family-level taxa (rows) for each mouse (columns). The abundance is shown as relative percentage. **f**, Relative abundance of select taxa. **g–i**, C57BL/6 mice were pretreated for 5 d with a cocktail of antibiotics (ampicillin, metronidazole, vancomycin and neomycin) added to the drinking water and then provided with water or 3% DSS-containing water for 6 d. On days 0, 2, 4 and 6, mice were orally administered with PBS or 30 mg kg^{-1} of HABN. On day 9, animals were euthanized and colon length (**g**), colonic damage scores (**h**) and colonic MPO activity (**i**) were measured. Data are presented as mean ± s.e.m. from a representative experiment ($n = 4$ biologically independent animals for PBS control groups in **g–i** and $n = 5$ biologically independent animals for all other panels) from four (**a–f**) and two (**g–i**) independent experiments. *$P < 0.05$, **$P < 0.01$, ***$P < 0.001$, ****$P < 0.0001$, analysed by one-way ANOVA with Tukey's HSD multiple comparison post hoc test.
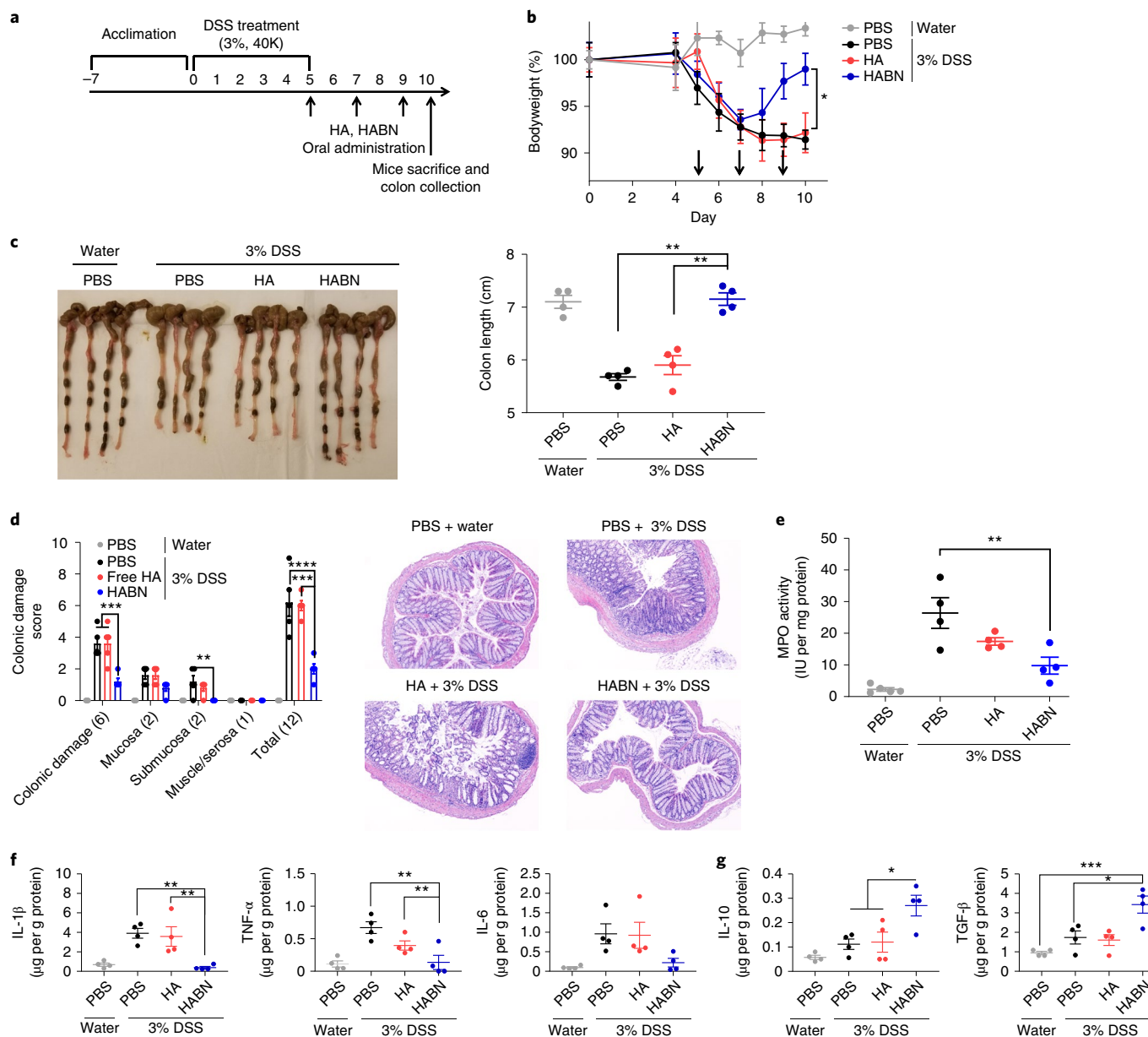
Fig. 5 | HABN alleviates colitis in a delayed therapeutic setting. a, C57BL/6 mice were provided with water or 3% DSS-containing water for 5 d. On days 5, 7 and 9, mice were orally administered with PBS or 30 mg kg⁻¹ of HA or HABN (with 100K HA at equivalent mass). **b**, Daily bodyweight changes in each group for 9 d. **c–g**, On day 9, animals were euthanized and colon length (**c**), colonic damage scores (**d**), colonic MPO activity (**e**) and local concentrations of pro-inflammatory (**f**) and anti-inflammatory (**g**) cytokines were quantitated. Data are presented as mean ± s.e.m. from a representative experiment ($n = 4$ biologically independent animals) from four independent experiments. *$P < 0.05$, **$P < 0.01$, ***$P < 0.001$ analysed by one-way (**c,e–g**) or two-way (**b,d**) ANOVA with Tukey's HSD multiple comparison post hoc test.

reduced efficacy of HABN against DSS-colitis ($P < 0.05$, compared to HABN without antibiotics, Fig. 4g–i and Supplementary Fig. 22), suggesting that the benefits of HABN are partially attributed to modulation of gut microbiome.

Amelioration of colitis after delayed treatment

Lastly, we examined the efficacy of HABN in a setting of delayed therapy. C57BL/6 mice were given 3% DSS in drinking water for 5 d and administered with HABN three times starting on day 5 (Fig. 5a). Within 3 d of initiating the HABN treatment, DSS mice started to recover bodyweight and by day 5 of HABN treatment (day 10 of the experiment) the animals were potently protected against

DSS-induced shortening of colon length, colonic damage and MPO activity (Fig. 5b–e). HABN treatment also suppressed the levels of IL-1β and TNF-α in colon while increasing the levels of anti-inflammatory IL-10 and TGF-β (Fig. 5f,g).

In summary, we have developed HABN with unique anti-inflammatory properties and demonstrated its therapeutic efficacy after oral administration in a murine model of acute colitis (Fig. 1a). While recent reports have explored systemic administration of polymer-modified BR for disease treatments[39–41], our work reported here demonstrates the promise of modulating intestinal barrier, microbiome and immune responses with orally administered HABN. We show that HABN accumulated in DSS-damaged

colonic epithelium and pro-inflammatory macrophages (Fig. 1e–g and Supplementary Figs. 10–12) and upregulated the expression levels of tight junction-associated proteins and antimicrobial peptides in colon, while restoring intestinal barrier functions and protecting the epithelial layer against apoptosis (Fig. 3a–e). Additionally, HABN treatment had a potent immune-modulatory impact in the lamina propria, characterized by significant decreases in pro-inflammatory cytokines and immune cells with concomitant increases in anti-inflammatory factors (Fig. 3f,g and Supplementary Fig. 19). Moreover, HABN promoted rapid recovery from body-weight loss, inhibited colon and mucosa damage, and decreased colonic MPO activity in the DSS murine model of acute colitis, whereas other control groups, including free HA mixed with bilirubin, HACN, as well as HAoxBR, failed to protect animals against colitis (Fig. 2 and Supplementary Fig. 16). In addition, PEG–BN, which had shown good efficacy against colitis after intravenous administration in a previous study[39], exerted only a moderate effect after oral administration in this study (Fig. 2), potentially due to the lack of HA-mediated targeting of inflamed colon. Importantly, HABN alleviated the symptoms of colitis more effectively than other conventional IBD therapies used in the clinic, such as 5-ASA, MPS and DEX (Fig. 2f–j). While adverse events, such as opportunistic infections, autoimmunity and liver toxicity, are associated with conventional immunosuppressive agents[6,10], we did not observe any overt toxicity after repeat HABN treatments, and HABN only transiently elevated local levels of anti-inflammatory IL-10 and TGF-β, which returned to the basal levels after stopping the HABN treatment (Supplementary Figs. 18 and 20). Taken together, these results show the efficacy and safety of HABN and demonstrate that both the HA shell and the BN core play critical and complementary roles in multi-faceted benefits of HABN against colitis.

HABN also altered the gut microbiome, increasing the diversity and relative abundance of *A. muciniphila, Clostridium* XIVα and *Lactobacillus* (Fig. 4). In particular, patients with IBDs have dramatically decreased abundance of *A. muciniphila*, known to promote mucus production and expression of tight junction proteins[25–27]; *Clostridium* XIVα whose metabolic byproduct, butyrate, induces T_{reg} cells in lamina propria[28]; and *Lactobacillus*, known to exert anti-inflammatory effects in both animal models of colitis[29–31] and patients with IBDs[32–35]. Notably, when we depleted commensal gut microbes with broad-spectrum oral antibiotics, HABN therapy partially lost its efficacy against DSS-colitis (Fig. 4g–i). While we speculate that the therapeutic efficacy of HABN was mediated in part by changes in the gut microbiome, further investigation is warranted to understand the role of altered microbiome on colitis. In addition, our current studies are limited to the mouse model of DSS-induced acute colitis, and validation in other advanced pre-clinical models of IBD is needed. Overall, these results suggest that ROS-responsive and hyaluronidase-resistant HABN accumulate in DSS-inflamed colon and protect colonic epithelium against inflammation while restoring disrupted intestinal barrier functions and gut microbiome.

It is increasingly recognized that the gut microbiome has a crucial role in human health, and the dysregulated microbiome has been implicated in a number of human diseases, including IBDs, obesity, diabetes, cancer and neurological disorders[3,42,43]. In particular, inorganic nanoparticles, such as silver nanoparticles widely used for their antimicrobial properties in consumer products and pharmaceutical products, have been shown to disrupt the gut microbiome, thus raising awareness of nanotoxicology and unintended outcomes of nanotechnology[44–46]. Whereas a recent study has reported a nanogel system that can overcome the dysregulated gut microbiome for vaccine applications in a mouse model of metabolic syndrome[47], our work represents a demonstration of oral nanomedicine capable of targeting inflamed colon and directly modulating the intestinal barrier and gut microbiota while exerting potent anti-inflammatory

responses against colitis. As dysregulated gut microbiota and intestinal barrier functions are highly associated with systemic diseases, our strategy described here may offer a convenient yet powerful platform for treatment of other inflammatory diseases.

Online content

Any methods, additional references, Nature Research reporting summaries, source data, statements of code and data availability and associated accession codes are available at https://doi.org/10.1038/s41563-019-0462-9.

References

1. Turner, J. R. Intestinal mucosal barrier function in health and disease. *Nat. Rev. Immunol.* **9**, 799–809 (2009).
2. Citi, S. Intestinal barriers protect against disease. *Science* **359**, 1097–1098 (2018).
3. Round, J. L. & Mazmanian, S. K. The gut microbiota shapes intestinal immune responses during health and disease. *Nat. Rev. Immunol.* **9**, 313–323 (2009).
4. Kostic, A. D., Xavier, R. J. & Gevers, D. The microbiome in inflammatory bowel disease: current status and the future ahead. *Gastroenterology* **146**, 1489–1499 (2014).
5. Halfvarson, J. et al. Dynamics of the human gut microbiome in inflammatory bowel disease. *Nat. Microbiol.* **2**, 17004 (2017).
6. Bernstein, C. N. et al. World gastroenterology organization practice guidelines for the diagnosis and management of IBD in 2010. *Inflamm. Bowel. Dis.* **16**, 112–124 (2010).
7. Lautenschlager, C., Schmidt, C., Fischer, D. & Stallmach, A. Drug delivery strategies in the therapy of inflammatory bowel disease. *Adv. Drug Deliv. Rev.* **71**, 58–76 (2014).
8. Wilson, D. S. et al. Orally delivered thioketal nanoparticles loaded with TNF-alpha-siRNA target inflammation and inhibit gene expression in the intestines. *Nat. Mater.* **9**, 923–928 (2010).
9. Zhang, S. et al. An inflammation-targeting hydrogel for local drug delivery in inflammatory bowel disease. *Sci. Transl. Med.* **7**, 300ra128 (2015).
10. Stallmach, A., Hagel, S. & Bruns, T. Adverse effects of biologics used for treating IBD. *Best Pract. Res. Clin. Gastroenterol.* **24**, 167–182 (2010).
11. Rayahin, J. E., Buhrman, J. S., Zhang, Y., Koh, T. J. & Gemeinhart, R. A. High and low molecular weight hyaluronic acid differentially influence macrophage activation. *ACS Biomater. Sci. Eng.* **1**, 481–493 (2015).
12. Hill, D. R., Kessler, S. P., Rho, H. K., Cowman, M. K. & de la Motte, C. A. Specific-sized hyaluronan fragments promote expression of human beta-defensin 2 in intestinal epithelium. *J. Biol. Chem.* **287**, 30610–30624 (2012).
13. Bollyky, P. L. et al. Intact extracellular matrix and the maintenance of immune tolerance: high molecular weight hyaluronan promotes persistence of induced CD4+CD25+ regulatory T cells. *J. Leukoc. Biol.* **86**, 567–572 (2009).
14. Zheng, L., Riehl, T. E. & Stenson, W. F. Regulation of colonic epithelial repair in mice by Toll-like receptors and hyaluronic acid. *Gastroenterology* **137**, 2041–2051 (2009).
15. Xiao, B. et al. Combination therapy for ulcerative colitis: orally targeted nanoparticles prevent mucosal damage and relieve inflammation. *Theranostics* **6**, 2250–2266 (2016).
16. Petrey, A. C. & de la Motte, C. A. Hyaluronan, a crucial regulator of inflammation. *Front. Immunol.* **5**, 101 (2014).
17. Kapitulnik, J. Bilirubin: an endogenous product of heme degradation with both cytotoxic and cytoprotective properties. *Mol. Pharmacol.* **66**, 773–779 (2004).
18. Sedlak, T. W. et al. Bilirubin and glutathione have complementary antioxidant and cytoprotective roles. *Proc. Natl Acad. Sci. USA* **106**, 5171–5176 (2009).
19. Chassaing, B., Aitken, J. D., Malleshappa, M. & Vijay-Kumar, M. Dextran sulfate sodium (DSS)-induced colitis in mice. *Curr. Protoc. Immunol.* **104**, 15.25.1–15.25.14 (2014).
20. Hansberry, D. R., Shah, K., Agarwal, P. & Agarwal, N. Fecal Myeloperoxidase as a Biomarker for Inflammatory Bowel Disease. *Cureus* **9**, e1004 (2017).
21. Hall, E. D., McCall, J. M., Chase, R. L., Yonkers, P. A. & Braughler, J. M. A nonglucocorticoid steroid analog of methylprednisolone duplicates its high-dose pharmacology in models of central nervous system trauma and neuronal membrane damage. *J. Pharmacol. Exp. Ther.* **242**, 137–142 (1987).
22. Li, B., Alli, R., Vogel, P. & Geiger, T. L. IL-10 modulates DSS-induced colitis through a macrophage-ROS-NO axis. *Mucosal Immunol.* **7**, 869–878 (2014).
23. Gibson, G. R. et al. Expert consensus document: the international scientific association for probiotics and prebiotics (ISAPP) consensus statement on the definition and scope of prebiotics. *Nat. Rev. Gastroenterol. Hepatol.* **14**, 491–502 (2017).

24. Ma, C. et al. Gut microbiome-mediated bile acid metabolism regulates liver cancer via NKT cells. *Science* **360**, eaan5931 (2018).
25. Cani, P. D. & de Vos, W. M. Next-generation beneficial microbes: the case of *Akkermansia muciniphila*. *Front. Microbiol.* **8**, 1765 (2017).
26. Everard, A. et al. Cross-talk between *Akkermansia muciniphila* and intestinal epithelium controls diet-induced obesity. *Proc. Natl Acad. Sci. USA* **110**, 9066–9071 (2013).
27. Zhang, Z. et al. Chlorogenic acid ameliorates experimental colitis by promoting growth of *Akkermansia* in mice. *Nutrients* **9**, 677 (2017).
28. Furusawa, Y. et al. Commensal microbe-derived butyrate induces the differentiation of colonic regulatory T cells. *Nature* **504**, 446–450 (2013).
29. Madsen, K. L., Doyle, J. S., Jewell, L. D., Tavernini, M. M. & Fedorak, R. N. Lactobacillus species prevents colitis in interleukin 10 gene-deficient mice. *Gastroenterology* **116**, 1107–1114 (1999).
30. Galdeano, C. M. & Perdigon, G. The probiotic bacterium Lactobacillus casei induces activation of the gut mucosal immune system through innate immunity. *Clin. Vaccine Immunol.* **13**, 219–226 (2006).
31. Geier, M. S., Butler, R. N., Giffard, P. M. & Howarth, G. S. Lactobacillus fermentum BR11, a potential new probiotic, alleviates symptoms of colitis induced by dextran sulfate sodium (DSS) in rats. *Int. J. Food Microbiol.* **114**, 267–274 (2007).
32. Sartor, R. B. Therapeutic manipulation of the enteric microflora in inflammatory bowel diseases: antibiotics, probiotics, and prebiotics. *Gastroenterology* **126**, 1620–1633 (2004).
33. Guandalini, S. Use of *Lactobacillus*-GG in paediatric Crohn's disease. *Dig. Liver Dis.* **34**, S63–S65 (2002). Suppl 2.
34. Zocco, M. A. et al. Efficacy of Lactobacillus GG in maintaining remission of ulcerative colitis. *Aliment Pharmacol. Ther.* **23**, 1567–1574 (2006).
35. Oliva, S. et al. Randomised clinical trial: the effectiveness of Lactobacillus reuteri ATCC 55730 rectal enema in children with active distal ulcerative colitis. *Aliment Pharmacol. Ther.* **35**, 327–334 (2012).
36. Png, C. W. et al. Mucolytic bacteria with increased prevalence in IBD mucosa augment in vitro utilization of mucin by other bacteria. *Am. J. Gastroenterol.* **105**, 2420–2428 (2010).
37. Fabia, R. et al. Impairment of bacterial flora in human ulcerative colitis and experimental colitis in the rat. *Digestion* **54**, 248–255 (1993).
38. Rakoff-Nahoum, S., Paglino, J., Eslami-Varzaneh, F., Edberg, S. & Medzhitov, R. Recognition of commensal microflora by toll-like receptors is required for intestinal homeostasis. *Cell* **118**, 229–241 (2004).
39. Lee, Y. et al. Bilirubin nanoparticles as a nanomedicine for anti-inflammation therapy. *Angew Chem. Int. Ed. Engl.* **55**, 7460–7463 (2016).
40. Kim, D. E. et al. Bilirubin nanoparticles ameliorate allergic lung inflammation in a mouse model of asthma. *Biomaterials* **140**, 37–44 (2017).
41. Lee, S., Lee, Y., Kim, H., Lee, D. Y. & Jon, S. Bilirubin nanoparticle-assisted delivery of a small molecule-drug conjugate for targeted cancer therapy. *Biomacromolecules* **19**, 2270–2277 (2018).
42. Cho, I. & Blaser, M. J. The human microbiome: at the interface of health and disease. *Nat. Rev. Genet.* **13**, 260–270 (2012).
43. Lynch, S. V. & Pedersen, O. The human intestinal microbiome in health and disease. *N. Engl. J. Med.* **375**, 2369–2379 (2016).
44. Pietroiusti, A., Magrini, A. & Campagnolo, L. New frontiers in nanotoxicology: gut microbiota/microbiome-mediated effects of engineered nanomaterials. *Toxicol. Appl. Pharmacol.* **299**, 90–95 (2016).
45. Javurek, A. B. et al. Gut dysbiosis and neurobehavioral alterations in rats exposed to silver nanoparticles. *Sci. Rep.* **7**, 2822 (2017).
46. Qiu, K., Durham, P. G. & Anselmo, A. C. Inorganic nanoparticles and the microbiome. *Nano Res.* **11**, 4936–4954 (2018).
47. Mosquera, M. J. et al. Immunomodulatory nanogels overcome restricted immunity in a murine model of gut microbiome-mediated metabolic syndrome. *Sci. Adv.* **5**, eaav9788 (2019).

Author contributions

Y.L. and J.M. designed the experiments. Y.L. performed all experiments. K.S. and N.K. contributed technical expertise, including qPCR analysis, LPMC isolation and flow cytometry analysis. Y.L. and J.M. analysed the data. M.G. aided with interpretation of data on gut microbiome analysis. S.J. contributed the initial design of bilirubin conjugates. Y.L. and J.M. wrote the paper.

Competing interests

The authors declare no competing interests.

Additional information

Supplementary information is available for this paper at https://doi.org/10.1038/s41563-019-0462-9.

Reprints and permissions information is available at www.nature.com/reprints.

Correspondence and requests for materials should be addressed to J.J.M.

Publisher's note: Springer Nature remains neutral with regard to jurisdictional claims in published maps and institutional affiliations.

Methods

Synthesis of HA−BR and HA−Chol conjugates. Before synthesizing HA−BR, an acid form of HA from HA sodium salt (Lifecore Biomedical) and an aminoethylene−bilirubin conjugate (AE−BR) were prepared. The acidic form of HA from HA sodium salt was prepared by dialysis against 0.01 M HCl overnight followed by lyophilization. AE−BR was prepared as previously described with modifications[48]. Briefly, 750 μmol of bilirubin (Lee Biosolutions) and 520 μmol of N-hydroxysuccinimide (NHS, Sigma-Aldrich) were added to 7.5 ml of dimethyl sulfoxide (DMSO) containing 0.225 μl of trimethylamine. Subsequently, 337.5 μmol of 1-ethyl-3-(3-dimethylaminopropyl)carbodiimide (EDC, Sigma-Aldrich) was added to the mixture. After stirring for 10 min at room temperature (RT), 562.5 μmol of ethylenediamine was added to the mixture, and the reaction was allowed to proceed with stirring for 4 h at RT under nitrogen gas. 50 ml of chloroform was added to the mixture and then washed twice with 50 ml of 0.1 M HCl, 0.1 M NaHCO$_3$ and then water. After evaporating the chloroform solution, 45 ml of methanol was added to the reaction mixture and then centrifuged at 3,000g for 10 min. The supernatant was then evaporated to yield AE−BR.

To synthesize HA−BR or HA−Chol conjugate, 80 μmol of an acidic form of HA and 40 μmol of NHS were added to 4.8 ml of DMSO and then, after adding 140 μmol of EDC, the mixture was stirred for 10 min at RT. Subsequently, 20 μmol of AE−BR or 5 μmol of cholesterol-PEG-NH$_2$ (Nanosoft Polymers) was added to the mixture overnight at RT under nitrogen gas. The mixture was slowly poured into 30 ml of 0.01 M NaOH and then dialysis was performed against 0.01 M NaOH for 5 h. Further dialysis was performed against a 1:1 ratio of water/acetonitrile three times for 1 d, followed by dialysis against distilled water three times for 2 d. The resulting solution was finally lyophilized, yielding HA−BR (native sodium salt form; 26.5 μg ml^{-1} of BR in 1 mg ml^{-1} of HABN) or HA−Chol. ^{1}H-NMR spectra were obtained on a Varian 500 MHz system (Varian); chemical shifts represent ppm downfield from tetramethylsilane. The bilirubin portion of HABN was calculated by measurement of ultraviolet/visible spectra using a Synergy NEO HTS multi-mode microplate reader (BioTek Instruments Inc).

Synthesis of PEG−BR. PEG−BR was prepared as previously described with modifications[48]. Here, 75 μmol of bilirubin and 33.75 μmol of EDC were added to 0.6 ml of DMSO containing 225 μl of trimethylamine and 52 μmol of NHS for 10 min at RT. Then, 15 μmol of polyethylene glycol 20K-amine (PEG-NH$_2$ Nanocs) was added, and the mixture was stirred for 4 h under nitrogen gas. Subsequently, the mixture was added to 50 ml of chloroform and then the organic solvents were washed by 50 ml of 0.1 M HCl twice, followed by washing with 50 ml of 0.1 M NaHCO$_3$ twice and finally washed with 50 ml of distilled water twice. The organic layer was evaporated and 50 ml of methanol was added to the residue. After centrifugation at 3,000g for 10 min, the supernatant was collected and then evaporated. Dialysis was performed as described in the previous section. To yield PEG−BR, lyophilization was performed. The final structure was confirmed by ^{1}H-NMR. ^{1}H-NMR spectra were recorded on a Varian 500 MHz system; chemical shifts represent ppm downfield from tetramethylsilane.

Synthesis of HA−Cy5.5, HA−Chol−Cy5.5 and HA−BR−Cy5.5 conjugates. Before conjugating HA−BR or HA−Chol with Cy5.5 amine (AAT Bioquest), a native sodium salt form of HA−BR, HA−Chol or free HA was converted into an acidic form of HA−BR, HA−Chol or free HA by dialysis processes for efficient dissolution to DMSO. Here 10 μmol of each power form was dissolved in 5 ml of distilled water. Dialysis was performed against 0.1 M HCl overnight and then the solution was dialysed against distilled water three times for 1 d. The resulting powder was obtained through a lyophilization step. Then 10.5 μmol of the acidic form of HA−BR, HA−Chol or free HA was dissolved in 0.8 ml of DMSO overnight. Then 2 μmol of NHS and 2 μmol of EDC were added to the mixture. After mixing for 10 min at RT, 0.1 μmol of Cy5.5-NH$_2$ was further added to the reaction mixture. After stirring overnight at RT, dialysis was performed against 0.01 M NaOH three times for 1 d, followed by dialysis against distilled water twice for 2 d. After lyophilization, the native sodium salt form of HA−Cy5.5, HA−Chol−Cy5.5 or HA−BR−Cy5.5 conjugate was obtained.

Preparation of Cy5.5-tagged HABN, HACN or PEG−BN nanoparticles. After dissolving HA−BR, HA−Chol, PEG−BR, HA−BR−Cy5.5 or HA−Chol-Cy5.5 in water or PBS, ultrasonication (140 W, 26 Hz, in short intervals of 2 s on and 3 s off) was performed for 5 min at 4 °C. After filtration through a 0.45 μm filter membrane, HABN, HACN, PEG−BN, HABN−Cy5.5 or HACN−Cy5.5 were acquired. The size and zeta potential of the nanoparticles were obtained using a Nanosizer ZS90 (Malvern Instruments Ltd). Morphology was examined by TEM using a JEOL 1400-plus transmission electron microscope (JEOL USA). The resulting nanoparticles were diluted in PBS or culture medium for in vitro and in vivo experiments.

ROS-responsiveness of 100K HABN and 100K HACN. 100K HABN or 100K HACN in PBS was incubated with or without a 100 mM solution of a peroxy radical-generating reagent AAPH (Sigma-Aldrich), 5 mM solution of hydrogen peroxide (H$_2$O$_2$, Sigma-Aldrich) or 1 mM solution of sodium hypochlorite (NaOCl, Sigma-Aldrich) for 1 h at 37 °C. The hydrodynamic size of the 100K HABN or

100K HACN were monitored at predetermined times by dynamic light scattering. The reaction was also monitored for 1 h by measuring absorbance at 453 nm using a Synergy NEO HTS multi-mode microplate reader.

Fluorescence measurement of dichlorofluorescin diacetate (DCFDA) on ROS and HABN. First, 50 μM of DCFDA in PBS was incubated with 1 mM of AAPH in the presence of BR (50 μM), HA (1 mg ml^{-1}), HABN (1 mg ml^{-1}) or PBS. Fluorescence signals of fluorescent 2′,7′-dichlorofluorescein (DCF) generated from DCFDA by oxidation were monitored for 1 h at 37 °C using a Synergy NEO HTS multi-mode microplate reader at 490 nm excitation and 520 nm emission.

Preparation of a native polymer form of oxidized HA−BR fragments (HAoxBR). For acquiring HAoxBR, 100K HABN in water was incubated with a 100 mM solution of AAPH for 1 h at 37 °C. After the reaction, the solution was centrifuged with a Amicon Ultra-Centrifugal filter with a membrane of 10 kDa at 17,500g at 4 °C for 15 min three times to remove the remaining AAPH. The filtered solution was lyophilized, to yield HAoxBR.

Colorimetric assessment of terminal N-acetyl-D-glucosamine (hyaluronan breakdown products). N-acetyl-D-glucosamine, a breakdown product of HA after exposure to hyaluronidase (HYAL), was measured using a colorimetric method described previously by Reissig et al.[49]. Briefly, 100K HABN (1 mg ml^{-1}) or 100K HA (1 mg ml^{-1}) in pH 6.0 PBS buffer was treated with 100 IU ml^{-1} of HYAL II (Sigma-Aldrich) at 37 °C for 6 h. 1 mg ml^{-1} of N-acetyl-D-glucosamine was used for the control group. At determined time points (0 h, 10 min, 0.5 h, 1 h, 2 h, 4 h and 6 h), 100 μl of the samples were taken, and the mixture was made up to 0.5 ml of PBS and heated for 5 min at 100 °C to stop the enzyme reaction. Then, 0.1 ml of 0.8 M potassium tetraborate (pH 9.0) was added to the mixture, which was further heated for 3 min at 100 °C and cooled in tap water. Then 3 ml of p-dimethylaminobenzaldehyde (DMAB) reagent (10 g of DMAB dissolved in 100 ml of glacial acetic acid containing 12.5% (v/v) of 10 M HCl) were added and, immediately after mixing, the tubes were placed in a water bath at 37 °C. After 20 min, the solution was measured at 544 nm wavelength using a Synergy NEO HTS multi-mode microplate reader.

Preparation of Nile Red-loaded 100K HABN. First, 10 μl of 1.5 mg ml^{-1} of Nile Red (Sigma-Aldrich) in methanol was added to 500 μl of 1 mg ml^{-1} of 100K HABN in water, and then ultrasonication (140 W, 26 Hz, in short intervals of 2 s on and 3 s off) was performed for 5 min at 4 °C. After moderate magnetic stirring overnight at RT to evaporate any remaining organic solvent, filtration through a 0.45 μm filter membrane was performed to remove the remaining unloaded aggregated Nile Red, yielding evenly sized Nile Red-loaded 100K HABN. The loaded amount of Nile Red in the nanoparticles was measured by high-performance liquid chromatography.

Animals. Animals were cared for following federal, state and local guidelines. All work performed on animals was in accordance with and approved by the Institutional Animal Care and Use Committee (IACUC) at University of Michigan, Ann Arbor. All animals were obtained from the Jackson Laboratory (Bar Harbor, ME) as mixed littermates and housed under pathogen-free conditions in the animal facility at the North Campus Research Complex of University of Michigan. Mice were cohoused for a week before random assignment to experimental groups to synchronize the gut microbiome among individual mice and reduce the heterogeneity of the gut microbiome[50]. The investigators were not blinded to allocation during experiments and outcome assessment, unless each section particularly included any blind assessment.

DSS-induced model of colitis. Six-week-old female C57BL/6 mice were housed in groups of five mice per cage and acclimatized for 1 week before inclusion in the study. Mice received 3% DSS (40 kDa; Alfa Aesar) supplemented in the drinking water for 5 or 6 d, followed by normal water. Control healthy mice were provided with normal water only. Then 30 mg kg^{-1} of HA (10 kDa, 100 kDa, 700 kDa or 1,500 kDa), 30 mg kg^{-1} of HAoxBR, 30 mg kg^{-1} of HABN (10 kDa, 100 kDa or 700 kDa), 30 mg kg^{-1} of PEG−BN, 30 mg kg^{-1} of HACN, HA+BR mixture (equivalent dose of HA and BR of HABN), 1 mg kg^{-1} of MPS, 1 mg kg^{-1} of DEX, 40 mg kg^{-1} of 5-ASA or PBS was administered via an oral route into mice on predetermined days. In some experiments, we pretreated mice by administering a cocktail of antibiotics (ampicillin 1 g l^{-1}, vancomycin 0.5 g l^{-1}, neomycin 1 g l^{-1} and metronidazole 1 g l^{-1}) in drinking water for 5 d before DSS treatment. Changes in bodyweight were assessed daily over the 9- or 10-d experimental period. Faeces were collected on the predetermined day for microbiome analysis. On the last day of the experiment, mice were sacrificed and the entire colon was excised. Colon length was measured and gently washed with physiological saline. Then, two pieces 0.5 cm in length of the distal section were used for histological assessment and immunofluorescence staining. The remaining colon tissue samples were used for fluorescence-activated cell sorting analysis and determining MPO activity and the concentrations of cytokines.

Histology. For histological analyses, hematoxylin and eosin (H&E) colonic tissue sections were prepared by the Unit for Laboratory Animal Medicine (ULAM)

In vivo Animal Core. Briefly, a 1 cm section of the distal colon was first fixed by incubation with 4% (v/v) buffered formalin and 70% (v/v) alcohol, and then embedded in paraffin. Tissue sections of the distal colon were then prepared, stained with H&E and analysed by Mantra quantitative pathology workstation (PerkinElmer). The severity of colonic histological damage was scored in a blinded fashion to prevent observer bias, as previously described[39]. Briefly, colonic damage was assigned scores as follows: 0, normal; 1, hyperproliferation, irregular crypts, and goblet cell loss; 2, mild to moderate crypt loss (10–50%); 3, severe crypt loss (50–90%); 4, complete crypt loss, surface epithelium intact; 5, small- to medium-sized ulcers (<10 crypt widths); 6, large ulcers (≥10 crypt widths). Inflammatory cell infiltration was scored separately for the mucosa (0, normal; 1, mild; 2, modest; 3, severe), submucosa (0, normal; 1, mild to modest; 2, severe) and muscle/serosa (0, normal; 1, moderate to severe). Scores for epithelial damage and inflammatory cell infiltration were summed, resulting in a total scoring range of 0 to 12.

MPO activity measurement. MPO activity was determined as previously described[39]. Briefly, a colon segment (1:10 w/v) in 50 mM phosphate buffer (pH 6.0) was homogenized using an IKA T25 ULTRA-TURRAX basic homogenizer (IKA Works, Inc.) at 4 °C. The colon suspension was 10-fold-diluted with 50 mM phosphate buffer containing 0.5% hexadecyltrimethylammonium bromide (Sigma-Aldrich). After sonicating for 10 s and subjecting to three freeze−thaw cycles, each sample was centrifuged at 17,000g for 5 min. Then 10 μl of each supernatant was added to 290 μl of 50 mM phosphate buffer (pH 6.0) containing 0.167 mg ml^{-1} of o-dianisidine dihydrochlrodie (Sigma) and 0.005% H_2O_2, and changes in absorbance at 460 nm were measured over 5 min. The protein concentration of the supernatant sample was measured using a Micro BCA Protein Assay Kit (Thermo Fisher Scientific). MPO activity was determined by comparison to a standard MPO curve (Sigma-Aldrich).

In vivo enzyme-linked immunosorbent assay (ELISA) analysis. For determining the concentrations of cytokines in the colon tissue, the colon segment in 50 mM phosphate buffer (pH 6.0) was homogenized (1:10 w/v) using an IKA T25 ULTRA-TURRAX basic homogenizer (IKA Works, Inc.) at 4 °C. Each sample was centrifuged for 10 min at 10,000g at 4 °C. The levels of cytokines in the resulting supernatants or medium were measured by ELISA at the Cancer Center Immunology Core of the University of Michigan.

In vivo immunofluorescence imaging. For acquiring in vivo confocal microscopy images, 5 cm of colon tissue was placed in Tissue-Tek optimum cutting temperature (OCT) cryomold blocks and transferred to a freezer at −70 °C. Tissue sections of the distal colon from the OCT-embedded frozen blocks were fixed with 4% para-formaldehyde (PFA), permeabilized with 0.1% or 0.25% Triton X-100 and blocked with phosphate buffered saline with Tween 20 (PBST) containing 1% or 3% BSA and 22.52 mg ml^{-1} of glycine. The sections were stained with 1 μg ml^{-1} of murine anti-beta defensin 3 (an orthologue of human beta-defensin 2) polygonal rabbit antibody for 1 h followed by 2 μg ml^{-1} of anti-rabbit secondary antibody conjugated with AlexaFluor-594, 5 μg ml^{-1} of anti-F4/80 antibody conjugated with AlexaFluor-488, 5 μg ml^{-1} of anti-beta-catenin antibody conjugated with AlexaFluor-594, 2 μg ml^{-1} of anti-EpCAM antibody conjugated with AlexaFluor-594, 5 μg ml^{-1} of anti ZO-1 antibody conjugated with AlexaFluor-488, and/or 1 μg ml^{-1} of anti occludin-1 antibody conjugated with AlexaFluor-594. Nuclei were counter-stained with Hoechst 33342. Images of random fields of view were acquired by confocal laser-scanning microscopy (Nikon A1; Nikon Instruments Inc). TUNEL assay was performed to detect apoptosis in OCT-embedded frozen blocks according to the manufacturer's instructions.

Quantitative reverse transcription PCR. RNA was extracted from colonic tissues using the E.Z.N.A. Total RNA Kit I (Omega Bio-tek) according to the manufacturer's protocol. Reverse transcription was performed using the High-Capacity cDNA Reverse Transcription Kit (Thermo Fisher Scientific). Quantitative PCR was performed with SYBR Green qPCR Kits (Alkali Scientific). The cycling conditions were 95 °C for 3 min and then 40 cycles of 95 °C for 15 s and 60 °C for 1 min. The relative expression of target genes was calculated using β-actin as a reference gene. The following primer sets were used for amplifications: ZO-1-Fw; 5′-CTTCTCTTGCTGGCCCTAAAC-3′, ZO-1-Rv; 5′-TGGCTTCACTTGAGGTTTCTG-3′, occludin-Fw; 5′-CACACTTGCTTGGGACAGAG-3′, occludin-Rv; 5′-TAGCCATAGCCTCC ATAGCC-3′, β-actin-Fw; 5′- AAGTGTGACGTTGACATCCG-3′, β-actin-Rv; and 5′- GATCCACATCTGCTGGAAGG -3′.

In vivo intestinal permeability assay. In vivo assay of intestinal permeability was performed using FITC-dextran, as described previously[19]. Briefly, mice were deprived of food and water for 4 h and then orally gavaged with 0.6 mg g^{-1} body weight of 4 kDa FITC-dextran (FD4, Sigma). Blood was collected retro-orbitally after 3 h, and FITC fluorescence intensity was measured in the serum samples (excitation, 485 nm; emission, 520 nm). FITC-dextran concentrations were determined using a standard curve generated by serial dilution of FITC-dextran in mouse serum.

Isolation of intestinal lamina propria mononuclear cells (LPMCs). Colon was removed and placed in cold Ca^{2+}, Mg^{2+}-free Hank's balanced salt solution (HBSS; Gibco). After removal of the mesentery, the colon was opened longitudinally, thoroughly washed in HBSS and cut into small pieces. The dissected mucosa was incubated with HBSS containing 1 mM dithiothreitol (Sigma-Aldrich) and 5 mM EDTA (Quality biological) for 30 min at 37 °C to remove the epithelial layer. The pieces of intestine were washed and placed in HBSS containing 1.5% foetal bovine serum (FBS), 200 U ml^{-1} collagenase Type 3 and 0.01 mg ml^{-1} DNase (all Worthington Biochemical Corporation) for 1 h at 37 °C. The digested tissues were washed, resuspended in 40% Percoll (GE Healthcare) and overlaid on a 75% Percoll fraction. Percoll gradient separation was performed by centrifugation at 700g for 20 min at RT. Mononuclear cells were collected at the interphase, washed and resuspended in staining buffer containing PBS, 0.5% BSA and 2 mM EDTA for flow cytometry or RPMI-1640 medium (Sigma-Aldrich) containing 10% FBS.

Flow cytometry. Cells were preincubated with a FcγR-blocking monoclonal antibody (CD16/32; 2.4G2, BD Bioscience) for 20 min followed by incubation with specific monoclonal antibodies for 20 min on ice. After staining surface molecules, the cells were resuspended in fixation/permeabilization solution (eBioscience), and intracellular staining of FOXP3 was performed with a FOXP3 staining buffer kit (eBioscience). Flow cytometric analyses were performed on a LSR II system (Becton Dickinson), and data were analysed using Flowjo software (Tree Star). Background fluorescence was assessed by staining with isotype-matched control monoclonal antibodies. FITC-, PE-, PerCP-Cy5.5-, APC-, PE-Cy7-, APC-Cy7- or AlexaFluor 647-conjugated monoclonal antibodies against CD4 (GK1.5), CD3 (145-2C11), CD11b (M1/70), CD11c (N148), Ly6c (HK1.4), MHCII (M5/114.15.2), 7AAD and FOXP3 (FJK-16S) were from eBioscience; CD45 (30-F11) and Ly6G (1A8) were from Invitrogen.

Microbiome analysis. One pellet of faeces was added to each well of PowerMag Glass Bead plate (Qiagen). The plate was properly packaged and shipped to the University of Michigan Medical School Host Microbiome Initiative (HMI) for microbiome analyses. Briefly, genomic DNA was extracted by using the Qiagen MagAttract Power Microbiome kit DNA/RNA kit (Qiagen, catalogue no. 27500-4-EP) on the EpMotion 5075 (Eppendorf) liquid handler. Extracted DNA was then used to generate 16S rRNA libraries for community analysis[51] using the MiSeq Illumina sequencing platform. Barcoded dual-index primers specific to the V4 region of the 16S rRNA gene were used for the construction.

Sequences were curated using the community-supported software program mothur (v.1.39)[52] and by following the steps outlined in the MiSeq SOP (http://www.mothur.org/wiki/MiSeq_SOP)[53]. Sequences were assigned to OTUs using a cut-off value of 0.03 and classified against the Ribosomal Database Project 16S rRNA gene training set (v.9) using a naive Bayesian approach with an 80% confidence threshold. Curated OTU sequence data were converted to relative abundance ± s.e.m. The Shannon diversity and inverse-Simpson indices were used to calculate alpha diversity, and the Yue and Clayton dissimilarity metric was used for beta diversity measures. Analysis of molecular variance was used to detect significant clustering of different treatment groups in non-metric multidimensional scaling. To confirm what specific bacterial taxa were over- and/or under-represented among groups, we analysed relative abundance results by using linear discriminant analysis effect size.

IVIS. To check ability of HABN to target the inflamed site in the colon, 1 d after preparing colitis mice or heathy mice by giving 3% DSS water or normal water for 5 d, 7.5 mg kg^{-1} of HABN−Cy5.5, HACN−Cy5.5 or HA−Cy5.5 (each containing 0.3% Cy5.5 w/w) was orally administered to the mice. After 6 h, mice were euthanized and organs including heart, kidney, lung, spleen, liver, stomach, small intestine and colon were excised. Fluorescence intensities in organs from each group were analysed using a Xenogen IVIS Lumina in vivo imaging system (PerkinElmer) with a Cy5.5 filter channel and an exposure time of 5 s.

Cell culture. J774A.1 murine macrophage and HT-29 colonic epithelial cell lines were obtained from the American Type Culture Collection (all cell lines were tested negative for mycoplasma contamination). J774A.1 cells or HT-29 cells in DMEM medium (Gibco) containing 10% (v/v) heat-inactivated FBS, 100 IU ml^{-1} penicillin/streptomycin and L-glutamine were cultured in a humidified 5% CO_2 atmosphere at 37 °C.

In vitro analysis of LPMCs. For the uptake study with LPMCs, LPMCs were isolated from the colon as described in Isolation of intestinal lamina propria mononuclear cells (LPMCs). LPMCs were cultured with 10 μg ml^{-1} of 100 K HABN−Cy5.5 for 3 h at 37 °C and then cells were preincubated with a FcγR-blocking mononuclear antibodies (CD16/32; 2.4G2, BD Bioscience) for 20 min, followed by incubation with specific mononuclear antibodies for 20 min on ice as detailed in Flow cytometry. Flow cytometric analyses were performed on a LSR II system and data were analysed using Flowjo software.

In vitro confocal microscopy. For the uptake study with the J774A.1 murine macrophage cell line, J774A.1 cells in culture medium were seeded onto cover

slips in 24-well plates (5×10^3 per well). After incubation for 2 d at 37 °C, the cells were treated with 100 ng ml^{-1} of lipopolysaccharide (LPS) and 10 ng ml^{-1} of IFN-γ for M1 induction, 20 ng ml^{-1} of IL-4 for M2 induction, or control medium. After 24 h, 5 µg ml^{-1} of 100K HABN−Cy5.5, 100 ng ml^{-1} of Nile Red, Nile Red-loaded 100K HABN (Nile Red, 100 ng ml^{-1}; 100K HABN 2.5 µg ml^{-1}) or control medium was treated with the cells for 1 h. The cells were then fixed with 4% PFA for 5 min, counter-stained with Hoechst 33342 for 10 min and analysed by confocal laser-scanning microscopy. For completion of the study, 5 mg ml^{-1} of free HA or 500 µg ml^{-1} of anti-CD44 antibody was pretreated with the cells for 30 min before nanoparticle treatment.

In vitro immunofluorescence imaging. For comparing β-defensin 2 levels on HT-29 colonic epithelial cells, HT-29 cells in culture medium were seeded onto 24-well plates (5×10^4 per well). After incubation for 2 d, 30 µg ml^{-1} of 100K HABN, 100K HA, 100K HACN, 20K PEG−BN or control medium were treated with the cells for 24 h. The cells were fixed and permeabilized with 4% PFA for 10 min and then 0.1% Triton X-100 for 10 min, blocked with PBST containing 3% BSA for 1 h, stained with anti-β-defensin 2 (human reactivity) rabbit polyclonal antibody (1 µg ml^{-1}) followed by 2 µg ml^{-1} of anti-rabbit IgG secondary antibody conjugated with AlexaFlour 488, and then counter-stained with Hoechst 33342. Images of random fields of view were acquired by confocal laser-scanning microscopy.

CCK-8 assay. HT-29 cells in culture medium were grown in 96-well plates (0.7×10^4 per well) for 24 h at 37 °C. After the medium was removed, fresh medium, H_2O_2 (100 µM) or different concentrations of HABN (500 µg ml^{-1}), HACN (500 µg ml^{-1}) and HA (500 µg ml^{-1}), with or without H_2O_2 (100 µM), was added to each well and plates were incubated for 24 h. After incubation, cells were washed with fresh culture medium and then 100 µl of fresh culture medium was added to each well, followed by the addition of 10 µl of CCK-8 (Dojindo Molecular Technologies, Inc.). After incubation for 1 h at 37 °C, the absorbance was measured at 450 nm using a 96-well plate microreader.

In vivo toxicity test. Six-week-old female C57BL/6 mice were housed in groups of five mice per cage and acclimatized for 1 week before inclusion in the study. Then 30 mg kg^{-1} of HABN (10 kDa, 100 kDa or 700 kDa) or PBS was administered via an oral route on day 0, 2, 4 and 6. Mice were observed over a 1-week period for changes in behaviour or weight. Blood was collected from the jugular vein and immediately sent to the ULAM Pathology Core for Animal Research for blind blood assessment. Mice were sacrificed and their major organs (heart, liver, lung, kidney, spleen and colon) were collected for histopathological analysis. Each organ was fixed with 4% (v/v) buffered formalin and 70% (v/v) alcohol, and embedded in paraffin. Tissues were sectioned, stained with H&E and examined by microscopy. All histological assessments were performed in a blinded manner to prevent observer bias.

Statistical analysis. All experiments were performed at least twice with duplicate repeated measures. The results are expressed as means ± s.e.m. A one-way or two-way analysis of variance (ANOVA), followed by Tukey's honestly significant difference (HSD) multiple comparison post hoc test was used for testing differences among groups. Data were approximately normally distributed and variance was similar between the groups. Experiments were repeated multiple times as independent experiments as indicated in the figure captions. Shown in each figure is a complete dataset from one representative, independent experiment. No samples were excluded from analysis. Statistical significance is indicated as *$P < 0.05$, **$P < 0.01$, ***$P < 0.001$ and ****$P < 0.0001$. GraphPad Prism v.6.0 (GraphPad Software) was used for statistical analyses.

Reporting Summary. Further information on research design is available in the Nature Research Reporting Summary linked to this article.

Data availability
The data supporting the findings of this study are available within the article and its Supplementary Information files. All relevant data can be provided by the authors upon reasonable request.

References
48. Lee, Y., Lee, S. & Jon, S. Biotinylated Bilirubin nanoparticles as a tumor microenvironment-responsive drug delivery system for targeted cancer therapy. *Adv. Sci. (Weinh.)* **5**, 1800017 (2018).
49. Reissig, J. L., Storminger, J. L. & Leloir, L. F. A modified colorimetric method for the estimation of *N*-acetylamino sugars. *J. Biol. Chem.* **217**, 959–966 (1955).
50. McCoy, K. D., Geuking, M. B. & Ronchi, F. Gut microbiome standardization in control and experimental mice. *Curr. Protoc. Immunol.* **117**, 23.1.1–23.1.13 (2017).
51. Seekatz, A. M. et al. Fecal microbiota transplantation eliminates *Clostridium difficile* in a murine model of relapsing disease. *Infect. Immun.* **83**, 3838–3846 (2015).
52. Schloss, P. D. et al. Introducing mothur: open-source, platform-independent, community-supported software for describing and comparing microbial communities. *Appl. Environ. Microbiol.* **75**, 7537–7541 (2009).
53. Kozich, J. J., Westcott, S. L., Baxter, N. T., Highlander, S. K. & Schloss, P. D. Development of a dual-index sequencing strategy and curation pipeline for analyzing amplicon sequence data on the MiSeq Illumina sequencing platform. *Appl. Environ. Microbiol.* **79**, 5112–5120 (2013).

nature research

Corresponding author(s): James J. Moon

Last updated by author(s): Jun 16, 2019

Reporting Summary

Nature Research wishes to improve the reproducibility of the work that we publish. This form provides structure for consistency and transparency in reporting. For further information on Nature Research policies, see <u>Authors & Referees</u> and the <u>Editorial Policy Checklist</u>.

Statistics

For all statistical analyses, confirm that the following items are present in the figure legend, table legend, main text, or Methods section.

n/a	Confirmed	
☐	☒	The exact sample size (n) for each experimental group/condition, given as a discrete number and unit of measurement
☐	☒	A statement on whether measurements were taken from distinct samples or whether the same sample was measured repeatedly
☐	☒	The statistical test(s) used AND whether they are one- or two-sided *Only common tests should be described solely by name; describe more complex techniques in the Methods section.*
☐	☒	A description of all covariates tested
☐	☒	A description of any assumptions or corrections, such as tests of normality and adjustment for multiple comparisons
☐	☒	A full description of the statistical parameters including central tendency (e.g. means) or other basic estimates (e.g. regression coefficient) AND variation (e.g. standard deviation) or associated estimates of uncertainty (e.g. confidence intervals)
☐	☒	For null hypothesis testing, the test statistic (e.g. F, t, r) with confidence intervals, effect sizes, degrees of freedom and P value noted *Give P values as exact values whenever suitable.*
☒	☐	For Bayesian analysis, information on the choice of priors and Markov chain Monte Carlo settings
☐	☒	For hierarchical and complex designs, identification of the appropriate level for tests and full reporting of outcomes
☐	☒	Estimates of effect sizes (e.g. Cohen's d, Pearson's r), indicating how they were calculated

Our web collection on <u>statistics for biologists</u> contains articles on many of the points above.

Software and code

Policy information about <u>availability of computer code</u>

Data collection	TEM images were acquired by AMT602 software. NMR spectra were acquired using VNMRJ software (v.4.0). Histology images were acquired using Matra Quantitative Pathology Workstation (v.1.0.3). Confocal fluorescence images were acquired by Nikon A1 NIS elements Imaging software (v.5.02). Flow cytomeric data were collected using BD FACSDiva (v.8.0.1). Microbiome data from feces were collected using the MiSeq Illumina sequencing platform. In vivo images were acquired using IVIS Lumina Living Image Software(v.4.5.5). Blood hematology and chemistry data were acquired using Hemavet 950 and Liasys 330, respectively.
Data analysis	NMR data spectra were analysed using MestReNova (v11.0). Histology images were analyzed by inForm image analysis software (v.2.3.0). Confocal fluorescence images were analyzed by Nikon A1 NIS elements Imaging software (v.5.02).Flow cytometry analysis was done in BD FACSDiva and FlowJo (v.10.5) (Tree Star). Microbiome analysis was done in the community-supported software program mothur (v.1.39) and by the steps in the MiSeq SOP (http://mothur.org/wiki/MiSeq_SOP). In vivo images were analyzed using IVIS Lumina Living Image (v.4.5.5) Software. Statistical analysis was done in GraphPad Prism 7.0.

For manuscripts utilizing custom algorithms or software that are central to the research but not yet described in published literature, software must be made available to editors/reviewers. We strongly encourage code deposition in a community repository (e.g. GitHub). See the Nature Research <u>guidelines for submitting code & software</u> for further information.

Data

Policy information about <u>availability of data</u>

All manuscripts must include a <u>data availability statement</u>. This statement should provide the following information, where applicable:

- Accession codes, unique identifiers, or web links for publicly available datasets
- A list of figures that have associated raw data
- A description of any restrictions on data availability

The authors declare that data supporting the findings of this study are available within the article and its Supplementary Information files. All relevant data can be provided by the authors upon reasonable request.

Field-specific reporting

Please select the one below that is the best fit for your research. If you are not sure, read the appropriate sections before making your selection.

☒ Life sciences　　☐ Behavioural & social sciences　　☐ Ecological, evolutionary & environmental sciences

For a reference copy of the document with all sections, see nature.com/documents/nr-reporting-summary-flat.pdf

Life sciences study design

All studies must disclose on these points even when the disclosure is negative.

Sample size	Sample sizes were chosen based on our preliminary data from at least two pilot experiments and previously published results in the literature.
Data exclusions	No data were excluded.
Replication	All experiments were repeated at least twice with similar results.
Randomization	Mice were assigned randomly to experimental groups based on body weights.
Blinding	Unless specifically mentioned in the Method section, the investigators were not blinded to allocation during experiments and outcome assessment since our data analyses are based on objectively measurable data.

Reporting for specific materials, systems and methods

We require information from authors about some types of materials, experimental systems and methods used in many studies. Here, indicate whether each material, system or method listed is relevant to your study. If you are not sure if a list item applies to your research, read the appropriate section before selecting a response.

Materials & experimental systems

n/a	Involved in the study
☐	☒ Antibodies
☐	☒ Eukaryotic cell lines
☒	☐ Palaeontology
☐	☒ Animals and other organisms
☒	☐ Human research participants
☒	☐ Clinical data

Methods

n/a	Involved in the study
☒	☐ ChIP-seq
☐	☒ Flow cytometry
☒	☐ MRI-based neuroimaging

Antibodies

Antibodies used	Immunofluorescence Experiments: Beta-defensin 3: Alpha Diagnostics, polygonal rabbit antibody, Cat#: MBD31-A, dilution 1:100 Anti-rabbit secondary antibody: Abcam Biochemicals, Cat#: ab175471(AlexaFlour-594), dilution 1:100 F4/80: Abcam Biochemicals, clone F4/80, Cat#: ab204266 (AlexaFluor-488), dilution 1:100 Beta-catenin: Abcam Biochemicals, clone E247, Cat#: ab201823 (AlexaFluor-594), dilution 1:100 Ep-CAM: Biolegend, clone G8.8, Cat#: 118222(AlexaFluor-594), dilution 1:250 ZO-1: Thermo Fisher Scientific, clone ZO1-1A12, Cat#: 339188 (AlexaFluor-488), dilution 1:100 Occludin-1: Thermo Fisher Scientific, clone OC-3F10, Cat#: 339188 (AlexaFluor-594), dilution 1:500 Flow Cytometry Experiements: CD4: eBioscience, clone GK1.5, Cat#: 11-0041-82 (FITC), dilution 1:100 CD3e: eBioscience, clone 145-2C11, Cat#: 45-0031-82 (PerCp-Cy5.5), dilution 1:100 CD11b: eBioscience, clone M1/70, Cat#: 11-0112-86 (FITC), dilution 1:100 CD11c: eBioscience, clone N418, Cat#: 25-0114-82 (PE-Cy7), dilution 1:100 Ly6C: eBioscience, clone HK1.4, Cat#:. 17-5932-82 (APC), dilution 1:100 MHCII, eBioscience, clone M5/114.15.2, Cat#: 48-5321-82, (eFluor 450), 1:200 FOXP3, eBioscience, clone FJK-16s, Cat#: 11-5773-82 (APC), 1:100 CD45, eBioscience, clone 30-F11, Cat#: 47-0451-82 (APC-Cy7), 1:200 Ly6G, eBioscience, clone 1A8, Cat#:.12-9668-80 (PE), 1:200 7AAD, eBioscience, 00-6993-50, dilution 1:100
Validation	Antibody validation was provided by manufacture's website (cell images) and/or data provided in the manuscript.

Eukaryotic cell lines

Policy information about cell lines

Cell line source(s)	J774A.1 murine macrophage and HT-29 colonic epithelial cell lines were obtained from the American Type Culture Collection (ATCC).
Authentication	J774A.1 and HT-29 were authenticated by ATCC.
Mycoplasma contamination	All cell lines were tested negative for mycoplasma contamination.
Commonly misidentified lines (See ICLAC register)	No commonly misidentified cell lines were used.

Animals and other organisms

Policy information about studies involving animals; ARRIVE guidelines recommended for reporting animal research

Laboratory animals	For in vivo studies, six-weeks old female C57-BL/6 mice were used. (Jackson Laboratory)
Wild animals	No wild animals were used.
Field-collected samples	No field-collected samples were used.
Ethics oversight	All work performed on animals was in accordance with and approved by the Institutional Animal Care & Use Committee (IACUC) at University of Michigan, Ann Arbor.

Note that full information on the approval of the study protocol must also be provided in the manuscript.

Flow Cytometry

Plots

Confirm that:

☒ The axis labels state the marker and fluorochrome used (e.g. CD4-FITC).

☒ The axis scales are clearly visible. Include numbers along axes only for bottom left plot of group (a 'group' is an analysis of identical markers).

☒ All plots are contour plots with outliers or pseudocolor plots.

☒ A numerical value for number of cells or percentage (with statistics) is provided.

Methodology

Sample preparation	The sample preparation was described in the Methods.
Instrument	BD Biosciences LSR II.
Software	FACSDiva was used for collection. FACSDiva and FlowJo were used for analysis.
Cell population abundance	Data on the abundance of relevant cell populations are provided in the manuscript.
Gating strategy	The cells were gated using the gating strategy as described in the Supplementary Information.

☒ Tick this box to confirm that a figure exemplifying the gating strategy is provided in the Supplementary Information.